Sample-detector coupling in atomic resolution magnetic resonance diffraction

Mladen Barbic[a] and Axel Scherer
Department of Applied Physics and Department of Electrical Engineering, M/S 200-36, California Institute of Technology, Pasadena, California 91125

(Received 19 June 2002; accepted 25 September 2002; publisher error corrected 18 April 2003)

A technique for potential realization of atomic resolution magnetic resonance diffraction was recently proposed for the case of a crystalline sample in proximity of a ferromagnetic sphere [M. Barbic, J. Appl. Phys. **91**, 9987 (2002)]. This article predicted the detection of distinct peaks in the number of resonant spin sites at different magnetic field values for specific sphere and crystal configurations. Here, the focus is on the specific detection coupling mechanisms between the resonant spin population of the sample and the magnetic sphere probe. We investigate and compare the force, torque, and flux detection mechanisms in order to provide guidance to the experimental efforts towards the realization of the atomic resolution magnetic resonance diffraction. We also investigate the dependence of the magnetic resonance diffraction spectrum on the relative position of the magnetic sphere with respect to the crystal lattice. © *2002 American Institute of Physics.* [DOI: 10.1063/1.1521795]

INTRODUCTION

Atomic resolution magnetic resonance diffraction has been desired ever since the introduction of magnetic resonance imaging (MRI) in two pioneering articles in 1973.[1,2] Since then, MRI has become an invaluable tool in medical science.[3] Although the inductive method of detection[4,5] has advanced the imaging resolution to the ~1-μm level,[6] the ultimate goal of achieving atomic resolution has remained elusive. In 1991, an alternative detection method for magnetic resonance imaging, magnetic resonance force microscopy (MRFM)[7] was proposed, with the ultimate goal of single spin sensitivity and three-dimensional (3D) imaging capability. The technique relies on the atomic scale imaging gradients from the microscopic magnetic particle mounted on a micromachined atomic force microscopy (AFM)-style mechanical cantilever for the appropriate detection sensitivity required for 3D single spin imaging.[8] Successful proof-of-concept MRFM demonstrations were reported for the cases of electron spin,[9] nuclear spin,[10] and ferromagnetic[11] resonance systems. MRFM research has benefited from the low-temperature implementations of the instrument,[12] and rapid advances in the fabrication techniques for incorporating smaller magnetic particles,[13,14] and more sensitive mechanical resonators.[15] However, reported MRFM imaging resolution of ~1 μm[16,17] remains at the level of inductive detection in conventional MRI.

We recently introduced a complementary magnetic resonance diffraction method[18] that significantly relaxes the challenging technical requirements of MRFM by allowing many spins to coherently contribute to the magnetic resonance signal, while still providing atomic scale information about the crystal structure of the sample. This approach closely resembles the initial magnetic resonance diffraction proposal[2,19] in which linear magnetic field gradients are used to selectively excite magnetic resonance in different atomic lattice planes. However, our approach differs from this original proposal by introducing nonlinear field gradients from a ferromagnetic sphere to achieve atomic resolution diffraction. The principles of the technique are briefly reviewed for the purpose of extending the analysis to include the appropriate experimental sample-detector coupling designs. A detailed description of the atomic resolution magnetic resonance diffraction using the magnetic fields from a ferromagnetic sphere is given in Ref. 18.

The inset of Fig. 1 shows the schematic representation of our diffraction method. A ferromagnetic sphere is placed in proximity of the surface of a simple cubic lattice crystal. Cobalt sphere with a magnetization per unit volume of 1500 emu/cm^3 is assumed to be 100 nm in diameter. The crystal is assumed to have a unit-cell size of $a_0 = 3$ Å. A large dc magnetic field B_0 is applied parallel to the sample surface in the z direction, polarizing the spins of the atomic lattice as well as saturating the magnetization of the ferromagnetic sphere. A small radio frequency field B_1 is applied perpendicular to the large polarizing dc magnetic field B_0. In the absence of the ferromagnetic sphere, the atomic spin sites in the crystal would experience the same externally applied field B_0 and therefore meet the magnetic resonance condition at the same magnetic resonance frequency ω_R. However, close to the ferromagnetic sphere, a large magnetic field gradient penetrates into the crystal, and only certain spin sites of the lattice satisfy the correct magnetic resonance conditions at any given magnetic field and frequency values. The magnetic field from the ferromagnetic sphere at point r in the sample has the following azimuthally symmetric dipolar form:

$$\vec{B}(\vec{r}) = \frac{3\vec{n}(\vec{m}\cdot\vec{n}) - \vec{m}}{|\vec{r}|^3}, \tag{1}$$

where n is the unit vector that points from the center of the

[a]Electronic mail: mladen@caltech.edu

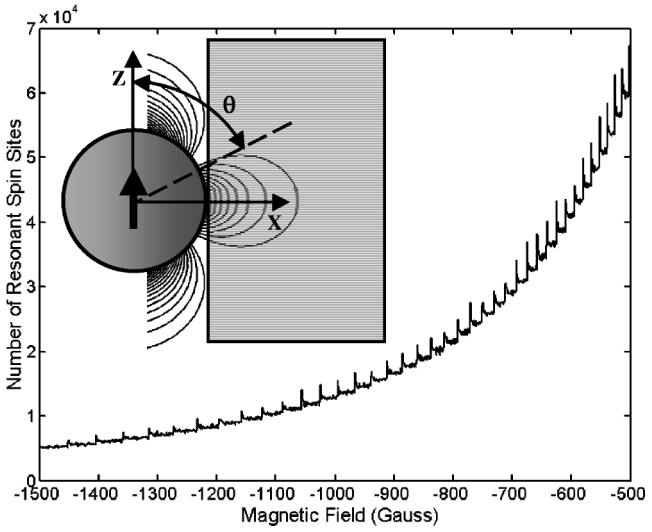

FIG. 1. Histogram of the number of resonant spin sites of the three-angstrom unit-cell size simple cubic crystal in the presence of a large polarizing field B_0 and the field from a 100 nm diameter cobalt ferromagnetic sphere. Inset shows the model configuration and the azimuthally symmetric contours of constant B_z.

ferromagnetic sphere to the crystal site location, and m is the magnetic moment vector of the sphere. The components of the ferromagnetic sphere magnetic fields (1) in the Cartesian coordinate system take the following form:

$$B_X(x,y,z)=\frac{3M_0\cdot x\cdot z}{(x^2+y^2+z^2)^{5/2}}, \tag{2}$$

$$B_Y(x,y,z)=\frac{3M_0\cdot y\cdot z}{(x^2+y^2+z^2)^{5/2}}, \tag{3}$$

$$B_Z(x,y,z)=\frac{M_0(2z^2-x^2-y^2)}{(x^2+y^2+z^2)^{5/2}}, \tag{4}$$

where M_0 is the magnitude of the saturation magnetic moment of the ferromagnetic sphere.

Due to the small size of the ferromagnetic sphere, the magnetic fields vary on the atomic scale and steps are taken in order to account for the discrete nature of the crystal lattice.[18] Labeling the atomic sites with indices (m,n,l), and assuming a unit-cell size with dimension a_0, the components in expressions (2–4) take the following form:

$$B_X(m,n,l)=\frac{3M_0\cdot m\cdot l}{a_0^3(m^2+n^2+l^2)^{5/2}}, \tag{5}$$

$$B_Y(m,n,l)=\frac{3M_0\cdot n\cdot l}{a_0^3(m^2+n^2+l^2)^{5/2}}, \tag{6}$$

$$B_Z(m,n,l)=\frac{M_0(2l^2-m^2-n^2)}{a_0^3(m^2+n^2+l^2)^{5/2}}, \tag{7}$$

where

$$m=\{167,168,...,+\infty\}$$
$$n=\{-\infty,\ldots,-1,0,+1,...,+\infty\},$$
$$l=\{-\infty,\ldots,-1,0,+1,...,+\infty\}$$

Since the external dc polarizing magnetic field B_0 is considered to be much larger than the field from the ferromagnetic sphere, only the z component of the magnetic field from the ferromagnetic sphere [Eq. (7)] is included when considering the resonant spins of the atomic lattice.[20] The contours of constant field B_z from the sphere are also shown in Fig. 1, and they have azimuthally symmetric form around the z axis. The index range for the x axis starts with integer value 167, since expressions (5)–(7) were derived for a 50-nm radius ferromagnetic sphere which is 166.66 times the lattice parameter of $a_0=3$ Å at the center of the coordinate system.

In the previous article,[18] a numerical summation was computed to construct a histogram of the number of resonant spin sites in the sample within a 1-G wide shell of constant B_z. This value of the bin width was selected since the linewidth broadening in solids is on the order of 1 G.[20] Distinct spectral peaks were discovered in the number of resonant spin sites with respect to the applied magnetic field in the negative value range, and Fig. 1 reproduces the spectrum between the field range of B_0-1500 G and B_0-500 G. Numerical simulations for the convolution of the force signal were previously reported by several MRFM research groups[21–23] using the integral expressions for a continuous medium sample. *However*, the positioning of the sample as shown in Fig. 1 (which is at 90° compared to the conventional MRFM configuration) and the explicit introduction into the model of the discrete nature of the atomic lattice sites allowed for the observation of the peaks in the magnetic resonance spectrum of Fig. 1. Such peaks would otherwise be obscured in the continuum sample model. The appearance of the magnetic resonance spectral peaks was therefore the *direct signature of the discrete atomic lattice sites*, and provides an opportunity to obtain direct atomic scale magnetic resonance information about a crystalline sample while detecting many lattice spins that are simultaneously in resonance at various magnetic field values.

The appearance of spectral peaks was explained using the 3D plots of the resonant spins under the influence of the polarizing magnetic field B_0 and the magnetic field from a ferromagnetic sphere.[18] Figure 2 shows two such representation plots for crystal lattice spin sites that are in resonance at the two adjacent magnetic field values. Only the positive values for the y-axis indices are plotted for clarity. At the lower magnetic field value of B_0-626 G, shown in Fig. 2(a), there are two empty regions at the top and bottom sections of the 1-G thin shell of constant B_z where no atomic spin sites are intersected. At this magnetic field value, the top and bottom sections of the shell of constant B_z from a ferromagnetic sphere are between the two crystal lattice planes, and do not intersect the atomic layers. At the magnetic field value of B_0-625 G, the location of one of the sharp resonant peaks in the spectrum of Fig. 1, the shell of constant B_z intersects the crystal lattice so that a large number of spin sites from the two lattice planes at the top and bottom sections of the resonant shell satisfy the resonance condition. The two bands of the resonant atoms from the lattice planes are clearly visible in Fig. 2(b), and the resonant ring bands like these at the distinct magnetic field values are responsible for the sharp peaks in the magnetic resonance spectrum. It is apparent then that the peaks in the magnetic resonance diffraction spectrum come from the region on the shell of constant B_z where

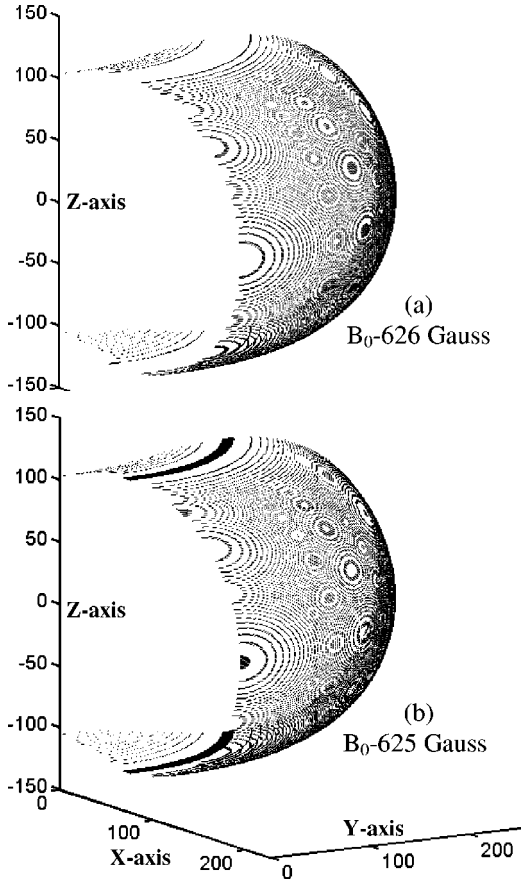

FIG. 2. Three-dimensional plots of the simultaneously resonant spin sites of the crystal lattice. At the magnetic field value of B_0-626 G in (a) two empty regions exist where the top and bottom of the shell of constant B_z are in between atomic lattice planes. At the magnetic field value of B_0-625 G in (b), the location of one of the spectral peaks in the spectrum of Fig. 1, the top and bottom sections of the shell of constant B_z intersect the two atomic lattice planes and are visible as the dark ring bands. These bands are responsible for the magnetic resonance diffraction effect.

$$\frac{\partial B_z}{\partial x}=\frac{\partial B_z}{\partial y}=0, \tag{8}$$

which, derived from Eq. (4), takes the following form:

$$\frac{3M_0x(x^2+y^2-4z^2)}{(x^2+y^2+z^2)^{7/2}}=\frac{3M_0y(x^2+y^2-4z^2)}{(x^2+y^2+z^2)^{7/2}}=0. \tag{9}$$

Therefore, the region of the shell of constant B_z responsible for the diffraction peak satisfies

$$x^2+y^2=4z^2, \tag{10}$$

which, when included in Eq. (4), describes the final condition for the location of the peaks in the magnetic resonance diffraction spectrum from the magnetic field of a ferromagnetic sphere

$$B_Z(z_l)=\frac{-2M_0}{(5)^{5/2}z_l^3}, \tag{11}$$

where $z_l=l\cdot a_0$.

The angle θ from the z axis where Eq. (8) is satisfied is $\theta=63.435°$.

FORCE DETECTED ATOMIC RESOLUTION MAGNETIC RESONANCE DIFFRACTION

Following the brief overview of the basic principles of atomic resolution magnetic resonance diffraction using a ferromagnetic sphere, we focus on the coupling of the resonant spins of the sample with the ferromagnetic sphere. The purpose of this investigation is to determine the detection method most appropriate for transcribing the spectral features of Fig. 1 into measurable signals in an experiment. The first potential method considered is to couple the ferromagnetic sphere through the force on the resonant spins of the sample. This is a natural detection choice, since most of the previous work on magnetic resonance imaging using ferromagnetic microparticles as gradient sources was performed by mechanical means with cantilever-type resonators. In addition, technical advancements in the resonant beam nanostructures have been extremely rapid,[24–27] and further sensitivity improvements are likely. Furthermore, integration of micron scale magnetic spheres into the probes of the cantilever resonators has already been demonstrated for other applications.[28,29] Therefore, many of the experimental challenges for implementation of atomic resolution magnetic resonance diffraction have been solved. Here, we predict the force values and spectral features in the experimental demonstration.

Force coupling of the spins with the ferromagnetic sphere is governed by the following relationship:

$$\vec{F}=\nabla(\vec{m}\cdot\vec{B}). \tag{12}$$

Written in the tensor format, this relationship takes the following form for the force on the resonant spin population of the sample at any given value of the applied field:

$$\begin{pmatrix}F_x\\F_y\\F_z\end{pmatrix}=\begin{pmatrix}\frac{\partial B_x}{\partial x} & \frac{\partial B_y}{\partial x} & \frac{\partial B_z}{\partial x}\\ \frac{\partial B_x}{\partial y} & \frac{\partial B_y}{\partial y} & \frac{\partial B_z}{\partial y}\\ \frac{\partial B_x}{\partial z} & \frac{\partial B_y}{\partial z} & \frac{\partial B_z}{\partial z}\end{pmatrix}\cdot\begin{pmatrix}m_x\\m_y\\m_z\end{pmatrix} \tag{13}$$

Since the externally applied polarizing magnetic field B_0 and the perpendicular high-frequency rf field B_1 are assumed to be uniform, the forces (which depend on the gradients of the magnetic field) on the resonant spin population do not depend on them. Therefore, only the nonuniform magnetic fields (5)–(7) from the ferromagnetic sphere need to be considered in the force calculations. It is emphasized that although only the z component of the total dc applied field was considered in order to determine the number and the location of the resonant spin sites of the sample, the force (13) on those resonant spins depends on the gradients of all three components (5)–(7) of the ferromagnetic sphere fields. Deri

vation of the tensor components in Eq. (13) with respect to the indices of the lattice sites (m,n,l) results in the following integer relationship for the total force on the sample:

$$\begin{pmatrix} F_x \\ F_y \\ F_z \end{pmatrix} = \sum_{m,n,l} \frac{3M_0}{a_0^4(m^2+n^2+l^2)^{7/2}} \begin{pmatrix} l(-4m^2+n^2+l^2) & -5m\cdot n\cdot l & m(m^2+n^2-4l^2) \\ -5m\cdot n\cdot l & l(m^2-4n^2+l^2) & n(m^2+n^2-4l^2) \\ m(m^2+n^2-4l^2) & n(m^2+n^2-4l^2) & l(3m^2+3n^2-2l^2) \end{pmatrix} \begin{pmatrix} m_x \\ m_y \\ m_z \end{pmatrix}. \tag{14}$$

In this expression, the total force on the sample at a particular value of the applied magnetic field is evaluated by summing over all of the integers (m,n,l) for which magnetic field value (7) is satisfied.

At this stage, it is helpful to consider the symmetry of the force tensor (14) with respect to the integer range of (m,n,l). It is apparent that many terms in the force tensor (14) are antisymmetric with respect to the positive and negative values of integers (n) and (l) that range from $-\infty$ to $+\infty$. Therefore, many tensor components in Eq. (14) sum to zero, and can be eliminated from the expression for the semi-infinite or thin-film samples

$$\begin{pmatrix} F_x \\ F_y \\ F_z \end{pmatrix} = \sum_{m,n,l} \frac{3M_0}{a_0^4(m^2+n^2+l^2)^{7/2}} \begin{pmatrix} 0 & 0 & m(m^2+n^2-4l^2) \\ 0 & 0 & 0 \\ m(m^2+n^2-4l^2) & 0 & 0 \end{pmatrix} \begin{pmatrix} m_x \\ m_y \\ m_z \end{pmatrix}. \tag{15}$$

It should be emphasized that this simplification of the force tensor is not allowed for cases where the integer range is not symmetric, such as for small crystallites[18] or samples with surfaces not parallel to the z axis.[18]

Figure 3 shows the calculation for the force in the x-axis direction according to the expression (15), using the value for the proton magnetic moment (CGS units) of $\mu_P = 1.4 \times 10^{-23}$ emu. The number spectrum of Fig. 1 is completely undetected in the force spectrum of Fig. 3. The explanation for this dramatic deflation is clear after rewriting expression (15) in the derivative form of expression (13) and noting that the two nonzero terms in Eq. (15) are equal

$$\begin{pmatrix} F_x \\ F_y \\ F_z \end{pmatrix} = \sum_{m,n,l} \begin{pmatrix} 0 & 0 & \frac{\partial B_z}{\partial x} \\ 0 & 0 & 0 \\ \frac{\partial B_z}{\partial x} & 0 & 0 \end{pmatrix} \begin{pmatrix} m_x \\ m_y \\ m_z \end{pmatrix}. \tag{16}$$

By examining this expression with respect to Eq. (8), it becomes apparent that the values of $\partial B_z/\partial x$ are *zero* or *approximately zero* at the top and bottom sections of the shells of constant B_z. Therefore, the force on the resonant spin sites that are responsible for the occurrence of the spectral peaks is negligible, and these spins do not contribute to the total force on the sample. As a result, for the cases of semi-infinite and thin-film crystalline samples, force detection is not appropriate for the experimental realization of the atomic resolution magnetic resonance diffraction, since it does not

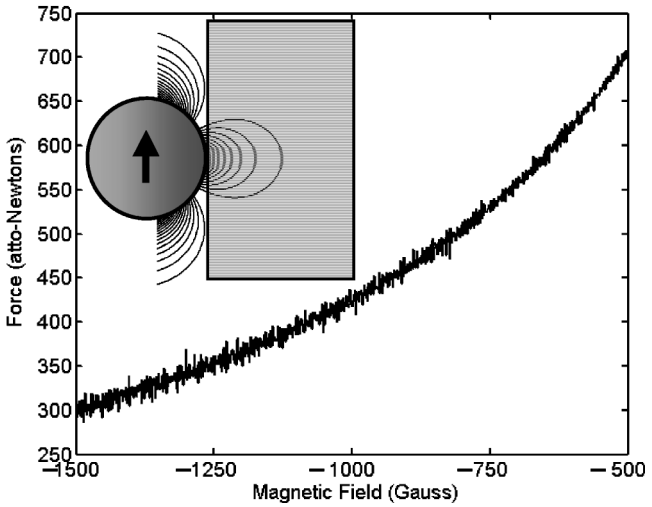

FIG. 3. Force spectrum for the x-direction detection, indicating that the spectral peaks of Fig. 1 are not revealed in the force measurement. The force on the resonant bands of Fig. 2(b) is negligible, therefore eliminating this detection method.

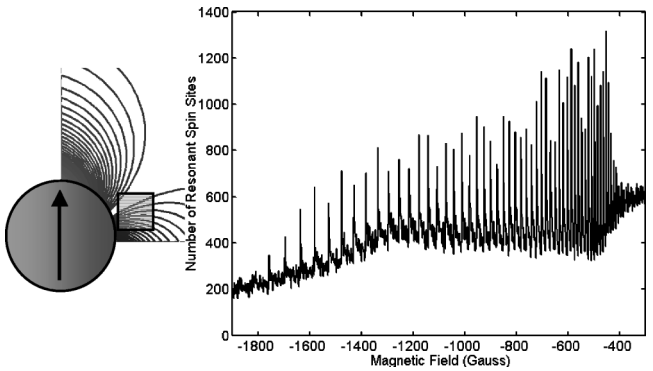

FIG. 4. Magnetic resonance histogram spectrum for a $100\times100\times100$ atoms crystallite with the simple cubic structure and three-Angstrom unit-cell size in the indicated configuration.

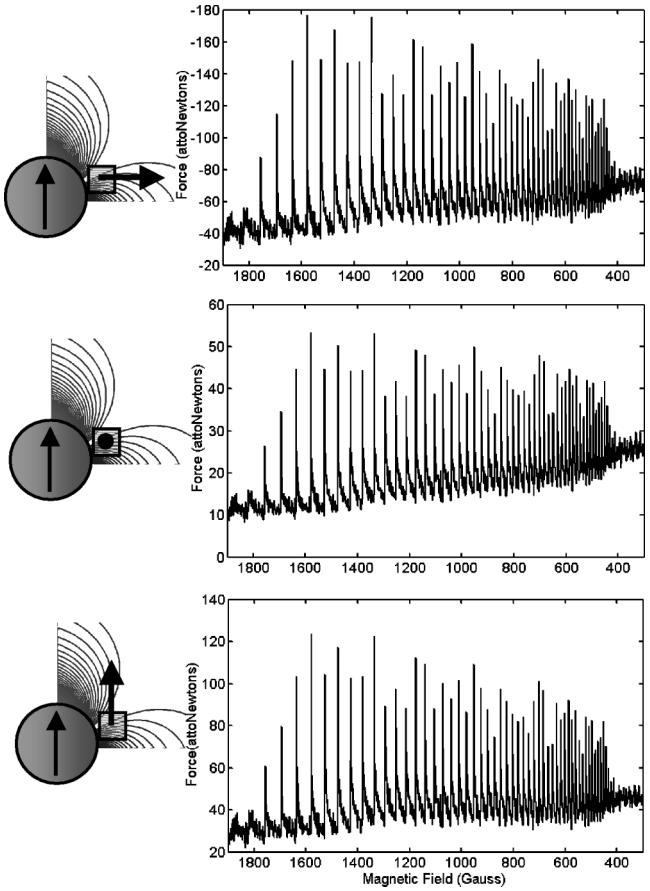

FIG. 5. Small crystallite force spectra for the three orthogonal detection axes. It is apparent that the transcription of the number spectrum of Fig. 4 is well represented in the magnetic resonance diffraction force spectra for all three detection axes.

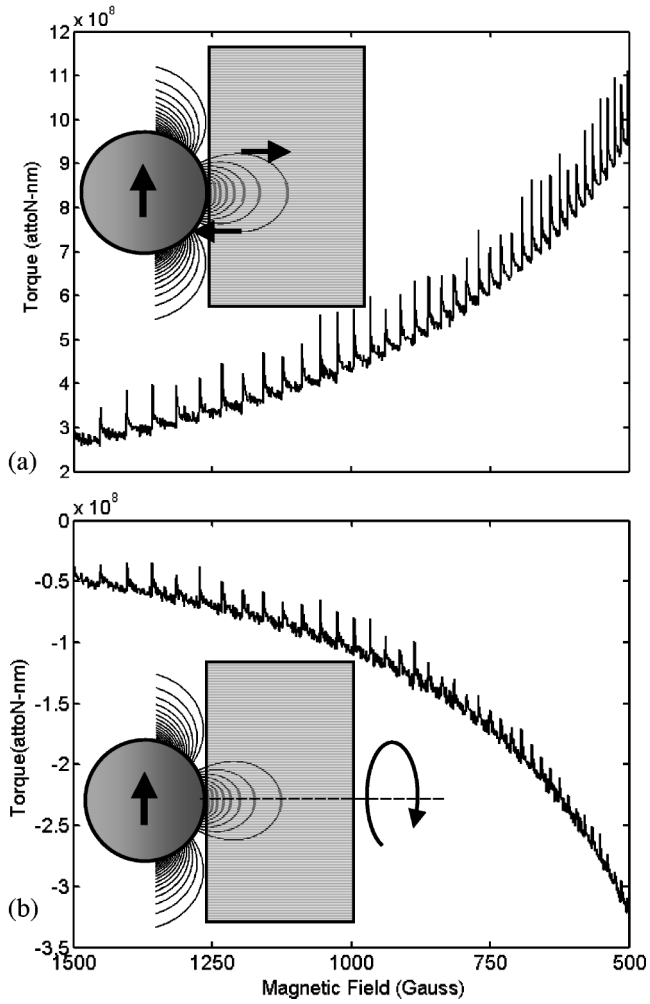

FIG. 6. The magnetic resonance diffraction torque spectra for the two axes of rotation. The torque around the y axis in (a) effectively amplifies the diffraction contrast, as the spectral features are stronger than in Fig. 1. The torque around the x axis in (b) shows a poor transcription of the spectral features of Fig. 1.

properly transcribe the distinct peaks in the number of resonant spin sites of Figs. 1 into the same or similar signatures in the force spectrum.

The force analysis yields a different result when considering a small crystallite. Figure 4(b) shows the number of resonant spin sites at different values of the magnetic field for a configuration shown in Fig. 4(a). In this configuration, a $100\times100\times100$ atom simple cubic lattice crystallite is positioned so that the spectral peaks are maximized in amplitude and contrast.[18] In this case, the index range of the force tensor (14) is not antisymmetric with respect to the Eq. (1) index range, while it remains antisymmetric with respect to the (n) index range for a crystallite centered with respect to the y axis. This results in the following tensor for force on a small crystallite, where the argument for the negligible force from the $\partial B_z/\partial x$ term in Eq. (16) have been included:

$$\begin{pmatrix} F_x \\ F_y \\ F_z \end{pmatrix} = \sum_{m,n,l} \frac{3M_0}{a_0^4(m^2+n^2+l^2)^{7/2}} \begin{pmatrix} l(-4m^2+n^2+l^2) & 0 & 0 \\ 0 & l(m^2-4n^2+l^2) & 0 \\ 0 & 0 & l(3m^2+3n^2-2l^2) \end{pmatrix} \begin{pmatrix} m_x \\ m_y \\ m_z \end{pmatrix} \tag{17}$$

Figure 5 shows the numerical calculation for the force on the resonant spins of a small crystallite for the three orthogonal axis. It is apparent that the transcription of the number spectrum of Fig. 4(b) is very well represented in the magnetic resonance diffraction force spectrum of Figs. 5(a)–5(c). The forces for the x axis and z axis are approximately three times and two times the force for the y axis, respectively. The expected forces of Fig. 5 on the protons of the crystallite of several hundred attonewtons are well above the force sensitivity limits previously demonstrated using microfabricated

cantilevers.[30] Therefore, force detection represents a viable route to atomic resolution magnetic resonance diffraction in small crystallites.

TORQUE DETECTED ATOMIC RESOLUTION MAGNETIC RESONANCE DIFFRACTION

The second potential method for the experimental measurement of atomic resolution magnetic resonance diffraction is torque detection. Whereas the force tensor (14) was shown to be antisymmetric for many matrix terms due to the positive and negative range of integers (n) and (l), resulting in the cancellation of the total force on the resonant spin population for the semi-infinite and thin-film samples, considerations of the mechanical torque on the sample reveal that the torque is nonzero for two axes of rotation. The inset of Fig. 6(a) shows an example for the first term $l(-4m^2+n^2+l^2)$ in the force tensor (14). For the resonant spins at the top of the shell of constant B_z, the force in the x direction is equal and opposite to the force on the spins at the bottom of the shell of constant B_z. Therefore, although the total force on the spin population is zero for this term in the force tensor matrix (14), the torque around the y axis is nonzero, and therefore needs to be considered as a viable route to experimentally demonstrating atomic resolution magnetic resonance diffraction.

The mechanical torque on the spin population at any given magnetic field value is governed by the following equation:

$$\vec{\Gamma}=\vec{F}\times\vec{r}. \tag{18}$$

Following the same steps of including the discrete nature of the crystal lattice, and substituting the force tensor (14) into the expression (18), a tensor expression is derived for the torque exerted on the spin population in terms of the integers (m,n,l)

$$\begin{pmatrix}\Gamma_x\\ \Gamma_y\\ \Gamma_z\end{pmatrix}=\sum_{m,n,l}\frac{3M_0}{a_0^3(m^2+n^2+l^2)^{5/2}}\begin{pmatrix}-m\cdot n & l^2-n^2 & -2n\cdot l\\ m^2-l^2 & m\cdot n & 2m\cdot l\\ n\cdot l & -m\cdot l & 0\end{pmatrix}\begin{pmatrix}m_x\\ m_y\\ m_z\end{pmatrix} \tag{19}$$

In this expression, the total torque on the sample at any given value of the z component of the magnetic field is evaluated by summing over all of the integers (m,n,l) for which expression (7) is satisfied.

Similar to the analysis for the force tensor (14), symmetry considerations are taken into account for the torque tensor (19) with respect to the index range of (m,n,l) for the semi-infinite and thin-film crystalline samples. Due to the cancellation of many terms, the torque tensor (19) significantly simplifies into the following expression:

$$\begin{pmatrix}\Gamma_x\\ \Gamma_y\\ \Gamma_z\end{pmatrix}=\sum_{m,n,l}\frac{3M_0}{a_0^3(m^2+n^2+l^2)^{5/2}}\begin{pmatrix}0 & l^2-n^2 & 0\\ m^2-l^2 & 0 & 0\\ 0 & 0 & 0\end{pmatrix}\begin{pmatrix}m_x\\ m_y\\ m_z\end{pmatrix}. \tag{20}$$

This expression reveals that the only nonzero terms in the tensor for the torque on the resonant spin populations are for the torques around the x axis and the y axis. These two torque terms are different, and Fig. 6 shows the numerical calculation for the two cases. The torque around the y axis, shown in Fig. 6(a), features a very high-spectral contrast. In fact, the spectral contrast in atomic resolution magnetic resonance diffraction using the torque detection method [Fig. 6(a)] is stronger than the predicted spectral contrast in the histogram of the number of resonant spin sites at various magnetic field values (Fig. 1). This means that the spins at the top and bottom of the shells of constant B_z (the ones responsible for the peaks in Fig. 1) exert more torque on the sample than the spins in the lobe of the shell of constant B_z (the ones that provide the background signal in Fig. 1). This feature in the torque detection method is very desirable as it effectively amplifies the atomic resolution magnetic resonance diffraction contrast. Figure 6(b) shows the numerical calculation for the torque on the sample around the x axis, and a very poor transcription of the diffraction spectrum of Fig. 1 into an appropriate torque spectral signature is observed. In addition, the values for the torque around the x axis in Fig. 6(b) are an order of magnitude smaller than the values expected for the y-axis torque of Fig. 6(a), and therefore represent an inferior axis in the torque detection of atomic resolution magnetic resonance diffraction. The development of the mechanical torque resonators over the last several decades[31–35] has been as rapid as the improvements in the cantilever-based force detectors, and therefore torque detection is also likely to be successful in the demonstration of atomic resolution magnetic resonance diffraction.

For the case of the torque detection of magnetic resonance diffraction in small crystallites, the torque term (19) reduces to

$$\begin{pmatrix} \Gamma_x \\ \Gamma_y \\ \Gamma_z \end{pmatrix} = \sum_{m,n,l} \frac{3M_0}{a_0^3(m^2+n^2+l^2)^{5/2}} \begin{pmatrix} 0 & l^2-n^2 & 0 \\ m^2-l^2 & 0 & 2m\cdot l \\ 0 & -m\cdot l & 0 \end{pmatrix} \begin{pmatrix} m_x \\ m_y \\ m_z \end{pmatrix}. \tag{21}$$

This expression is similar to Eq. (20), and indicates that the torque detection of atomic resolution magnetic resonance diffraction should also be successfully observed for a small crystallite case.

In addition to the forces and torques on the sample that result in the predicted experimental signatures of atomic resolution magnetic resonance diffraction, additional measurement methods may achieve predicted spectral features. Several nonimaging cantilever-type experiments have been reported that rely on the direct transfer of angular momentum[36,37] and energy[38,39] to the spin population in magnetic resonance. Such experiments have demonstrated similar sensitivity to the initial demonstrations of imaging-type, cantilever-detected magnetic resonance, and therefore also represent possible routes to atomic resolution magnetic resonance diffraction demonstration. The simplicity in these nonimaging cantilever detected magnetic resonance experiments derives from the principle that all of the resonant spins in the sample are detected equally. Therefore, in this class of experiments, the expected spectral features are the same as the ones shown in Figs. 1 and 4.

FLUX DETECTED ATOMIC RESOLUTION MAGNETIC RESONANCE DIFFRACTION

Although cantilever-based detection of magnetic resonance represents a viable route to the demonstration of atomic resolution magnetic resonance diffraction, inductive detection techniques should not be overlooked, especially in lieu of the constant improvements in the sensitivity of the more traditional magnetic resonance detectors. These include microcoil NMR,[40] superconducting quantum interference device (SQUID) detectors,[41] Hall sensors,[42] and superconducting resonators,[43] which collectively represent a flux-detection class of magnetic resonance measurement methods. These sensors have benefited from advances in microfabrication resulting in micron-scale conducting loops,[44] Hall sensors,[45,46] and SQUID detectors.[47] Furthermore, they have been implemented into the probes intended for imaging by raster scanning.[48–52] They may also have additional advantages when compared to the force detectors with regard to the linearity of the probe-detector coupling.[53]

For the case of atomic resolution magnetic resonance diffraction, a circular pick-up loop is considered for the capture of the magnetic flux from the resonant spins of the crystalline sample, as shown in Fig. 7. The flux from a spin captured by the loop is[8]

$$\Phi_P = \mu_P \left(\frac{\mu_0}{2\pi}\right) \frac{\pi}{r_{\text{loop}}}, \tag{22}$$

where $\mu_0 = 4\pi \times 10^{-7}$, and the diameter of the loop is taken to be 1 μm and centered around the ferromagnetic sphere. This loop diameter is still larger than the $\sim$100 nm^3 sample volume that is being interrogated in this diffraction technique. Therefore, it is assumed that all of the resonant spins in the sample are detected equally. The total captured flux spectrum in atomic resolution magnetic resonance diffraction is therefore equal to the spectrum of Fig. 1 but modified by the multiplication factor (22), which for a proton spin is equal to $\Phi_P = 0.85 \times 10^{-11} \Phi_0$, where Φ_0 is the flux quantum $\Phi_0 = 2.067 \times 10^{-7}$ G cm^2. Since the number of spins detected at any magnetic field value in Fig. 1 is on the order of 10^4, the total flux captured by a 1-μm loop is on the order of $\Phi \sim 1 \times 10^{-7} \Phi_0$. This is still a challenging number, but it presents us with a metric for future flux detector development for atomic resolution magnetic resonance diffraction. It is also noted that this calculation was performed for the case of a pickup loop much larger than the sample region being investigated. Further reduction in the pickup loop size improves the flux detection efficiency and in turn increases the value of the magnetic flux captured by the loop. However, the simple analytical expression for the captured flux (22) for a spin centered inside the pickup loop would have to be replaced by exact modeling of the flux detector shape and the relative position with respect to the resonant spins of the sample. Analytical expressions for the magnetic field from a circular loop over all space exist[54] and could be used in conjunction with the principle of reciprocity[55,56] to determine precisely the spin-detector coupling in the flux detection of atomic resolution magnetic resonance diffraction. The loop configurations, and the noncircular flux detectors such as Hall probes, are subjects of a further study.

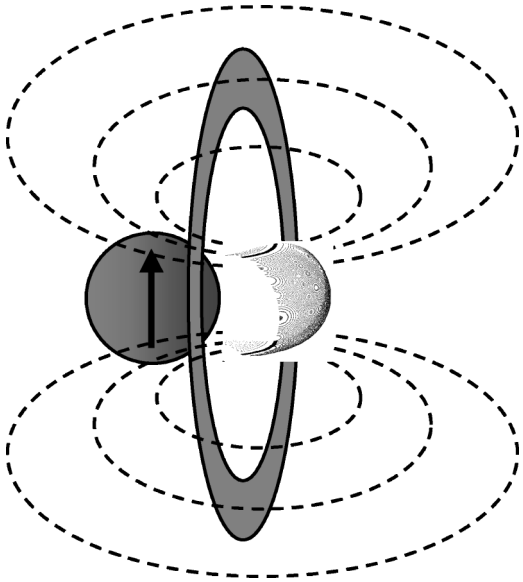

FIG. 7. Schematic diagram for the flux detection of atomic resolution magnetic resonance diffraction. In this configuration, the magnetic flux from the x component of the resonant magnetic moments of the sample is detected.

In all sample-detector coupling schemes in atomic resolution magnetic resonance diffraction described so far, no mention has been made of the magnetic resonance signal modulation schemes. Such ac modulation techniques would probably have to be employed for successful experimental demonstration, especially if the resonant detector, such as a mechanical cantilever in magnetic resonance force microscopy, is used. Several ac modulation techniques in force detection of magnetic resonance have either already been demonstrated, such as cyclic saturation[9] and cyclic adiabatic rapid passage,[10] or are under investigation, such as spin precession detection.[8] These advances are certain to accelerate experimental realization of atomic resolution magnetic resonance diffraction.

POSITIONING SENSITIVITY IN ATOMIC RESOLUTION MAGNETIC RESONANCE DIFFRACTION

In the analysis of the atomic resolution magnetic resonance diffraction, we also consider the sensitivity of the spectral peak features on the relative positioning of the ferromagnetic sphere with respect to the crystal lattice. Figure 2(b) already described the reasoning behind the appearance of the distinct spectral peaks, with the two wide bands at the top and bottom of the shell of constant B_z being responsible for the diffraction pattern. This visualization also helps describe the positioning sensitivity of this diffraction method. It is apparent from Fig. 2(b) that there will not be any significant shift in the diffraction spectrum of Fig. 1 with the small displacement of the sphere in the y direction since the shells of constant B_z still properly intersect the same atomic lattice planes. A similar conclusion can be drawn about the translation of the sphere with respect to the x axis. As the sphere is retracted from the sample in the x direction, the shells of constant B_z still intersect the lattice planes sufficiently deeply that the distinguishable sharp peaks in the spectrum appear even for a sphere retraction by 10 nm. The case is more complex for the sphere positioning in the z direction. Figure 8(a) shows the spectrum for the ferromagnetic sphere centered at one of the lattice planes, while Fig. 8(b) shows the spectrum for the ferromagnetic sphere centered in between the two lattice planes. The two spectra are offset by half the distance between two spectral peaks. This is not a surprising result, as the shift in the ferromagnetic sphere position also shifts the field values at which the atomic planes are resonant. The magnetic fields from the ferromagnetic sphere vary on the atomic scale and are responsible for obtaining magnetic resonance diffraction peaks in the first place. The shift of the sphere position in the z direction will therefore strongly influence the spectral peak position.

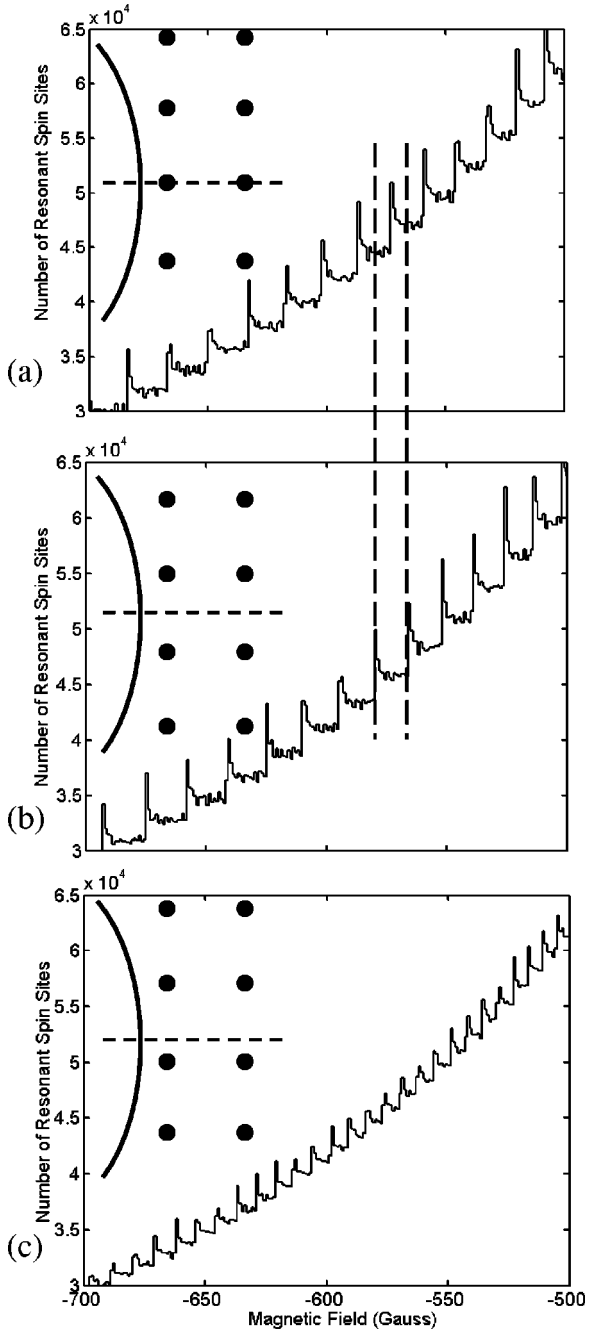

FIG. 8. The histogram spectrum in (a) for the sphere centered at one of the lattice planes, while (b) shows the spectrum for the sphere centered in between the two lattice planes. The spectra are offset by half the distance between adjacent spectral peaks, as the shift in the sphere position shifts the field values at which the atomic planes are resonant. Figure 8(c) shows the spectrum for the sphere offset from the center position by one quarter of the lattice spacing in the z direction resulting in the doubling of the number of spectral peaks and lowering of the amplitudes of spectral peaks.

Figure 8(c) shows the spectrum for the ferromagnetic sphere being offset from the center position by one quarter of the lattice spacing in the z direction. One then observes doubling of the number of spectral peaks in the diffraction spectrum, as well as lowering of the amplitudes of the spectral peaks. This observation is again best explained through the use of the 3D visualization of the resonant spin sites of the lattice at specific values of the magnetic field. Figures 9(a) and 9(b) show the 3D representation plots of the simultaneously resonant spin sites at the two magnetic field values of the adjacent spectral peaks in the spectrum of Fig. 8(c). In this asymmetric sphere position, the atomic lattice planes are not intersected simultaneously at the top and bottom of the shell of constant B_z, but at two different magnetic field values. At the lower magnetic field value of B_0-628 G shown in Fig. 9(a), only one atomic plane is intersected at the bottom of the shell of constant B_z. At the location of the next spectral peak in the spectrum of Fig. 8(c) at B_0-620 G, shown in

Fig. 9(b), the shell of constant B_z intersects another single atomic lattice plane, this time at the top of the shell. Therefore, due to these alternating resonant atomic planes at the top and bottom of shells of constant B_z, the number of spins in a spectral peak is halved, and the number of the peaks in the spectrum is doubled. This analysis for the sphere versus crystal lattice positioning relationship means that the experimental setup for the demonstration of atomic resolution magnetic resonance diffraction will have to maintain a subangstrom positioning precision, a feat achieved in most high-performance scanning tunneling microscopy and atomic force microscopy instruments.[57–60]

Such an analysis naturally leads to the question whether it would be possible to amplify the magnetic resonance diffraction spectrum signal by dispersing a large number of monosized ferromagnetic spheres onto a flat crystal surface, and measuring a collective signal from such an array. Recent advances in the synthesis of nanoscopic monodisperse ferromagnetic spheres have been truly remarkable,[61–64]

[31] R. N. Kleiman, G. K. Kaminsky, J. D. Reppy, R. Pindak, and D. J. Bishop, Rev. Sci. Instrum. **56**, 2088 (1985).
[32] R. N. Kleiman, G. Agnolet, and D. J. Bishop, Phys. Rev. Lett. **59**, 2079 (1987).
[33] A. N. Cleland and M. L. Roukes, Nature (London) **392**, 160 (1998).
[34] C. A. Bolle, V. Aksyuk, F. Pardo, P. L. Gammel, E. Zeldov, E. Bucher, R. Boie, D. J. Bishop, and D. R. Nelson, Nature (London) **399**, 43 (1999).
[35] D. W. Carr, S. Evoy, L. Sekaric, H. G. Craighead, and J. M. Parpia, Appl. Phys. Lett. **77**, 1545 (2000).
[36] C. Ascoli, P. Baschieri, C. Frediani, L. Lenci, M. Martinelli, G. Alzetta, R. M. Celli, and L. Pardi, Appl. Phys. Lett. **69**, 3920 (1996).
[37] M. Lohndorf, J. Moreland, and P. Kabos, Appl. Phys. Lett. **76**, 1176 (2000).
[38] J. Moreland, M. Lohndorf, P. Kabos, and R. D. McMichael, Rev. Sci. Instrum. **71**, 3099 (2000).
[39] A. Jander, J. Moreland, and P. Kabos, Appl. Phys. Lett. **78**, 2348 (2001).
[40] D. L. Olson, T. L. Peck, A. G. Webb, R. L. Magin, and J. V. Sweedler, Science **270**, 1967 (1995).
[41] L. R. Narasimhan, C. K. N. Patel, and M. B. Ketchen, IEEE Trans. Appl. Supercond. **9**, 3503 (1999).
[42] G. Boero, P. A. Besse, and R. Popovic, Appl. Phys. Lett. **79**, 1498 (2001).
[43] R. D. Black, T. A. Early, P. B. Roemer, O. M. Mueller, A. Mogro-Campero, L. G. Turner, and G. A. Johnson, Science **259**, 793 (1993).
[44] L. Kong and S. Y. Chou, Appl. Phys. Lett. **70**, 1474 (1997).
[45] M. L. Roukes, A. Scherer, S. J. Allen, Jr., H. G. Craighead, R. M. Ruthen, E. D. Beebe, and J. P. Harbison, Phys. Rev. Lett. **59**, 3011 (1987).
[46] A. K. Geim, S. V. Dubonos, J. G. S. Lok, I. V. Grigorieva, J. C. Maan, L. T. Hansen, and P, E. Lindelof, Appl. Phys. Lett. **71**, 2379 (1997).
[47] W. Wernsdorfer, B. Doudin, D. Mailly, K. Hasselbach, A. Benoit, J. Meier, J.-Ph. Ansermet, and B. Barbara, Phys. Rev. Lett. **77**, 1873 (1996).
[48] V. Agrawal, P. Neuzil, and D. W. van der Weide, Appl. Phys. Lett. **71**, 2343 (1997).
[49] A. M. Chang, H. D. Hallen, L. Harriott, H. F. Hess, H. L. Kao, J. Kwo, R. E. Miller, R. Wolfe, J. van der Ziel, and T. Y. Chang, Appl. Phys. Lett. **61**, 1974 (1992).
[50] A. Oral, S. J. Bending, and M. Henini, Appl. Phys. Lett. **69**, 1324 (1996).
[51] T. Schweinbock, D. Weiss, M. Lipinski, and K. Eberl, J. Appl. Phys. **87**, 6496 (2000).
[52] J. R. Kirtley, M. B. Ketchen, K. G. Stawiasz, J. Z. Sun, W. J. Gallagher, S. H. Blanton, and S. J. Wind, Appl. Phys. Lett. **66**, 1138 (1995).
[53] H. Bergh and E. W. McFarland, Meas. Sci. Technol. **7**, 1019 (1996).
[54] L. D. Landau, E. M. Lifshitz, and L. P. Pitaevskii, *Electrodynamics of Continuous Media*, 2nd ed. (Pergamon Press, Oxford, 1980).
[55] A. Aharoni, *Introduction to the Theory of Ferromagnetism* (Oxford University, New York, 1996).
[56] W. F. Brown, *Magnetostatic Principles in Ferromagnetism* (North-Holland, Amsterdam, 1962).
[57] G. Binning, H. Rohrer, C. Gerber, and E. Weibel, Phys. Rev. Lett. **49**, 57 (1982).
[58] G. Binning, C. F. Quate, and C. Gerber, Phys. Rev. Lett. **56**, 930 (1986).
[59] D. M. Eigler and E. K. Schweizer, Nature (London) **344**, 524 (1990).
[60] F. J. Giessibl, S. Hembacher, H. Bielefeldt, and J. Mannhart, Science **289**, 422 (2000).
[61] C. Petit, A. Taleb, and M. P. Pileni, Adv. Mater. **10**, 259 (1998).
[62] S. Sun, C. B. Murray, D. Weller, L. Folks, and A. Moser, Science **287**, 1989 (2000).
[63] A. F. Puntes, K. M. Krishnan, and A. P. Alivisatos, Science **291**, 2115 (2001).
[64] T. Hyeon, S. S. Lee, J. Park, Y. Chung, and H. B. Na, J. Am. Chem. Soc. **123**, 12798 (2001).
[65] J. A. Stratton, *Electromagnetic Theory* (McGraw-Hill, New York, 1941).